DALTON
FULL PAPER

Structural characterisation of new Ru^{II}[9]aneS_3 polypyridylic complexes †

João Madureira,[a] Teresa M. Santos,[a] Brian J. Goodfellow,[a] Mónica Lucena,[a] Júlio Pedrosa de Jesus,[a] Maria G. Santana-Marques,[a] Michael G. B. Drew[b] and Vítor Félix *[a]

[a] *Department of Chemistry, University of Aveiro, 3810-193 Aveiro, Portugal*
[b] *Department of Chemistry, The University, Whiteknights, Reading, UK RG6 6AD*

Received 14th June 2000, Accepted 27th September 2000
First published as an Advance Article on the web 6th November 2000

A large number of new $[Ru^{II}([9]aneS_3)(L)Cl]^+$ complexes (where L is a polypyridyl bidentate ligand) were synthesized from the precursor $[Ru([9]aneS_3)(dmso)Cl_2]$ in the search for new DNA intercalators. The ancillary ligands used have different molecular architectures which include cross bridges, pyridyl units, phenanthroline and diamine derivatives. The related complex $[Ru([9]aneS_3)(ind)Cl_2]$, containing the monodentate ligand indazole, was also prepared. The diimine complexes $[Ru([9]aneS_3)(pdi)Cl]^+$ and $[Ru([9]aneS_3)(phi)Cl]^+$ were prepared *in situ* from the ligands pda (*o*-phenylenediamine) and dap (phenanthrene-9,10-diamine), respectively, *via* Ru assisted amine/imine oxidation. All complexes were characterised through ^{1}H NMR, IR, UV-Vis and electrospray mass spectrometry. Furthermore, the PF_6 salts of seven $[Ru([9]aneS_3)(L)Cl]^+$ and $[Ru([9]aneS_3)(dip)Cl]BF_4$ (dip = 4,7-diphenylphenanthroline) have been investigated by X-ray single crystal diffraction. The crystal structures are presented and analysed in terms of the molecular assemblies of the complex cations and anions and the molecular hydrogen bonding interactions. The π-stacking geometric arrangements of the extended aromatic systems dppz (dipyrido[3,2-*a*:2′,3′-*c*]phenazine) and dip in their metal complexes are also discussed.

Introduction

One of the major areas of research involving ruthenium polypyridyl complexes is in RNA/DNA recognition.[1] Typically, these complexes show non-covalent (electrostatic) interactions in the exterior of the DNA helix, groove-bound association (direct hydrogen bonding or van der Waals interactions with the nucleobases in the groove) and intercalation (stacking interactions between nucleobases and aromatic ligands). Prototypes have included $[Ru(bpy)_2L]^{2+}$ or $[Ru(phen)_2L]^{2+}$, where L is a polypyridyl able to interact non-covalently with DNA.

The choice of the metal centre and the macrocycle ancillary ligand followed several criteria in order to try and achieve goals, such as anti-tumor action and improvement of the selectivity and specificity of the intermolecular interactions between DNA and the metal complexes. Ruthenium(II) is an excellent candidate: it is known that ruthenium(III) anti-tumor complexes are reduced *in vivo* to Ru^{II}, the state with cytotoxic activity,[2] and as Ru^{II} is diamagnetic (d^6) metal complex–DNA interaction studies can be monitored easily by NMR. Polypyridyls such as 1,10-phenanthroline and 2,2′-bipyridyl have been the usual choice as ancillary ligands, if only non-covalent metal complex-DNA interactions are required.[1,3] The use of macrocyclic complexes has several advantages over all polypyridylic systems. Macrocyclic polyamines have been used in the synthesis of complexes with transition metals and lanthanides for sensory and diagnostic applications and several reviews have appeared recently.[4,5] In contrast to complexes containing "ancillary" ligands such as phenanthrolines, thia- or aza-crowns are able to form hydrogen bonds and specific van der Waals contacts with the functional groups of DNA bases located in the major groove.[6a] Also a fully polypyridylic co-ordination sphere results in much greater steric hindrance on binding to DNA, when compared to thioether macrocycles, limiting intercalation to open structures in the major groove.[7] Moreover, complexes with macrocyclic ligands, compared to those with only polypyridyls, offer the advantage of minimisation of optical isomerism.[8] In this context the complexes $[Rh([12]aneN_4)(phi)]^{3+}$ and $[Rh([12]aneS_4)(phi)]^{3+}$ (phi = 9,10-phenathrenequinone diimine), synthesized by Barton and co-workers, represent two successful examples of metal systems containing both macrocyclic and polypyridylic ligands used in the DNA-complex interaction studies.[1,6] Searching for new DNA intercalators, our group has been involved in the study of new ruthenium(II) complexes with polythioether macrocycles and polypyridyls, or related N-heterocyclic ligands.[9]

The symmetric macrocycle [9]aneS_3 (1,4,7-trithiacyclononane) was chosen in order to synthesize octahedral complexes, of the type $[Ru^{II}([9]aneS_3)(L)Cl]^+$ (where L is a polypyridyl bidentate ligand) which are able to interact non-covalently with DNA. Additionally, the presence of a labile chloride in the metal co-ordination sphere allows the possibility of covalent bonding.[7]

Phenanthroline and bipyridyl derivatives, presented in Scheme 1, form rigid five membered chelate rings upon co-ordination with metal ions. Furthermore their aromatic surfaces can be extended to turn them into good candidates for intercalation with nucleobases, since there is experimental evidence that stacking free energy correlates reasonably well with the surface area of the ligand.[10] The best known examples of this class of compounds are dppz (dipyrido[3,2-*a*:2′,3′-*c*]-phenazine)[11] and phi.[6,12,13] Cross-bridged pyridyl ligands (dipa, dpk, dpm) offer other possibilities such as the formation of six membered rings that are more flexible than phen or bpy derivatives. The bridging group is an important variable since it influences the co-ordination mode of the ligand and as well as the structural and optical properties of the complex.[14,15] These ligands may be used in DNA–complex interactions as

† Electronic supplementary information (ESI) available: ES-MS spectra, crystal packing diagrams, syntheses of complexes, ligand conformations, hydrogen bond parameters, crystal data, analytical and spectroscopic data for complexes. See http://www.rsc.org/suppdata/dt/b0/b004752j/

 DOI: 10.1039/b004752j

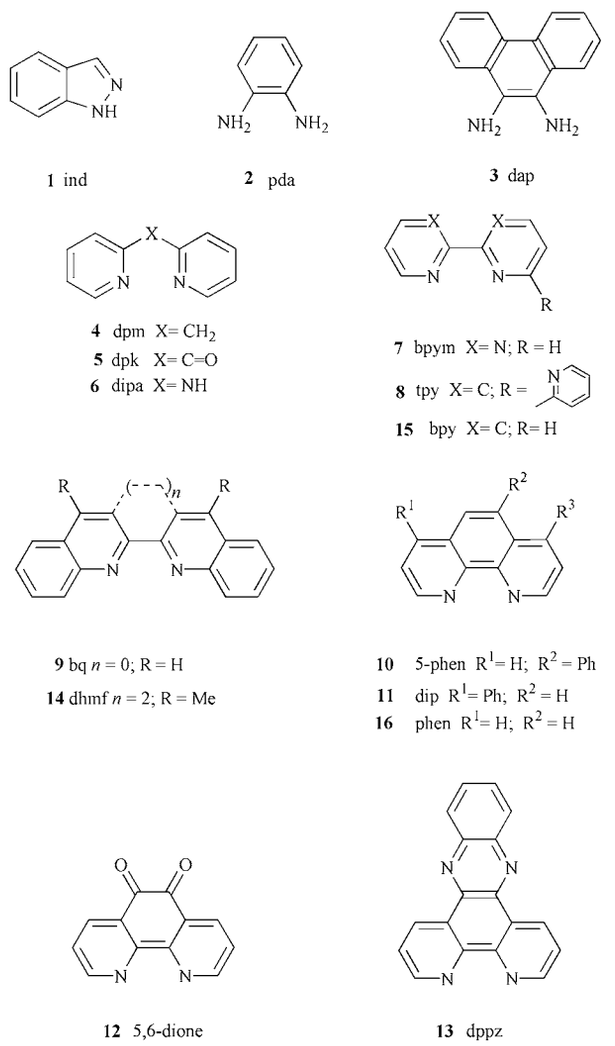

Scheme 1

carboplatin [diammine(cyclobutanedicarboxylato)platinum(II)] analogues[16,17] and other ligands can be covalently added at the bridging atom opening new pathways for intercalative ligand synthesis.

In this study the synthesis and structural characterisation of a large number of Ru^{II}/[9]aneS_3 and polypyridyl complexes are presented. The complexes have been characterised using a plethora of techniques including ^{1}H NMR, infrared spectroscopy, UV/Vis, electrospray mass spectrometry and X-ray single crystal diffraction. For simplicity all complex cations and their corresponding neutral species are labelled similarly (the polypyridyl ligands are shown in Scheme 1).

Results and discussion

Synthesis and characterisation

All Ru^{II}/[9]aneS_3/polypyridyl complexes reported in this study were synthesized according to the method described previously[9a] which consists of a simple substitution reaction of dmso and a Cl ligand in the [Ru([9]aneS_3)(dmso)Cl_2] precursor complex by a bidentate polypyridyl ligand. The experimental details and full structural data of all the complexes reported are given as ESI supplementary material. The supplementary tables and figures are indicated by the letter S.

Complex **1** with a monodentate ind ligand was prepared with two Cl ligands resulting in a neutral species. This complex is very insoluble in most solvents and slightly soluble in dmso. Electrospray, ^{1}H NMR and UV-Vis spectra were therefore recorded in this solvent. The ES mass spectrum shows peaks at *m*/*z* 513, 435 and 407 which can be assigned to the [Ru([9]-aneS_3)(ind)(dmso)Cl]$^+$, [Ru([9]aneS_3)(ind)Cl]$^+$ and [Ru([9]-aneS_3)(ind)Cl − CH_2CH_2]$^+$ cations respectively. The first cation is formed during dissolution of **1** with dmso by replacement of a labile chloride ion. The other two ions are formed by dmso loss and by joint losses of dmso and CH_2CH_2 from the macrocycle, respectively. The NMR spectrum of the complex exhibits changes with time typical of a complex undergoing substitution in agreement with the ES data. Owing to the complexity of the spectra only the H^3 peak of the ind ligand was used to follow appearance and disappearance of the various species. The H^3 peak of free ind was identified at δ 8.05 (5% after 20 min) and the bi-substituted form, [Ru([9]aneS_3)(ind)$(dmso)_2$]$^{2+}$ at δ 8.59. This bi-substituted form is still present in solution after one month (30%) and is favoured by an increase in temperature (70% after 4 h at 40 °C). The neutral form, [Ru([9]aneS_3)(ind)-Cl_2], has a peak at δ 8.40 and the monosubstituted [Ru([9]-aneS_3)(ind)Cl(dmso)]$^+$ shows two peaks at δ 8.13 and 8.50 probably due to the existence of two optical isomers.

The complexes [Ru([9]aneS_3)(pdi)Cl]$^+$ **2** and [Ru([9]aneS_3)-(phi)Cl]$^+$ **3** were obtained *in situ* from pda and dap ligands, respectively, *via* Ru-assisted amine/imine oxidation (see Scheme 2).[6b,18] In fact complex **2** shows three characteristic IR bands

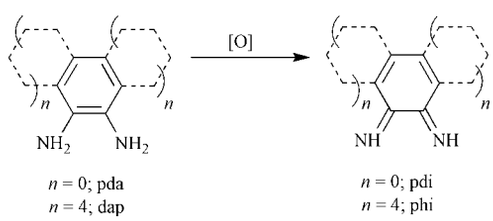

Scheme 2

at 1523 ($\delta_{N\text{-}H}$ bending), 1451 and 1378 cm^{-1} characteristic of co-ordinated pdi.[18a] However the expected sharp band at 3280–3300 cm^{-1} for co-ordinated pdi[18a,f,19] appears as a strong and broad $\nu_{N\text{-}H}$ band between 3250 and 2800 cm^{-1}. Since all free pda amine vibrations ($\nu_{asN\text{-}H}$ (3385s), $\nu_{sN\text{-}H}$ (3346s), $\delta_{N\text{-}H}$ (1632s), $\nu_{C\text{-}N}$ (1274s), $\omega_{N\text{-}H}$ (910–660 s,br cm^{-1})) are absent in the IR spectrum, the presence of the imine form in complex **2** is clearly demonstrated. The IR spectrum of complex **3** shows characteristic vibrations of co-ordinated phi,[18a] namely the medium intensity band at 1497 cm^{-1} ($\delta_{N\text{-}H}$), the C=N vibration at 1602 cm^{-1} and the sharp =N–H peaks at 3318 and 3208 cm^{-1}. Furthermore the ES mass spectral patterns obtained for **2** and **3** are those expected for the corresponding complexes with the reduced forms of co-ordinated pdi and phi instead of pda and dap. The comparison presented in Fig. S1 between the simulated spectrum of [Ru([9]aneS_3)(dap)Cl]$^+$ and the experimental spectrum of complex **3** shows that the spectra differ in two mass units showing unequivocally that the oxidation of dap to the phi diimine form occurs.[18a,e,f] The oxidation of pda to pdi in the preparation of complex [Ru([9]aneS_3)(pdi)Cl]$^+$ **2** was also investigated by ^{1}H NMR spectroscopy. In order to check for the presence of the NH protons, spectra in water–D_2O (9 : 1) were recorded. Two peaks at δ 12.68 and 12.60 were present and the integration of these and the aromatic protons gave the correct stoichiometry. The presence of two peaks suggests, as for other Cl containing complexes, that the labile Cl is being replaced by H_2O giving a mixture of two complexes. This effect is only seen for the NH protons and not for the aromatic protons (less delocalisation). Confirmation of this is given by ^{1}H NMR spectrum of **2** in methanol (a non-co-ordinating solvent) where only one NH resonance is seen. For complex **3** one peak is seen for the two NH protons in CD_3CN owing to C_2 symmetry.

The IR spectrum of complex [Ru([9]aneS_3)(dpk)Cl]$^+$ **5** shows two bands at 1673 and 1306 cm^{-1}, characteristic of the carbonyl group and assigned to the vibrational modes $\nu_{C=O}$ and $\delta_{C\text{-}(C=O)\text{-}C}$ respectively. The presence of these bands and the absence of diol or hemiketal C–O bands ($\nu_{sC\text{-}O\text{-}C}$ at 1275–1200 and $\nu_{asC\text{-}O\text{-}C}$

at 1075–1020 cm^{-1}) is clear evidence that the bridging carbonyl retains its double bond character. This result is also consistent with the crystal structure found for this complex (see below). The C=O bond length is 1.244(41) Å and the angles centred at the carbon of the carbonyl group C–C–O are 115.3(41) and 126.9(52)°, and the C–C–C angle is 113.40(38)°, which agrees with those reported for free dpk (C=O 1.215 Å, C–C–O 119.9 and 120.4 and C–C–C 119.7°).[20] This result is surprising since the synthesis of **5** was carried out in ethanol. It is well known that when dpk is co-ordinated to a metal centre the carbonyl group usually suffers nucleophilic addition of alcohol or water from the solvent and subsequent re-hybridisation of the carbon atom from sp^2 to sp^3.[21] The change in stereochemistry of the bridging carbon leads to a significant decrease in the steric strain of the six-membered chelate ring thus favouring nucleophilic attack. In most of the known dpk complexes, characterised by X-ray diffraction, the ligand appears as a diol, hemiketal or ketal.[22] There are only a few examples of dpk complexes where the carbonyl bridge retains its double bond character.[22]

The IR spectrum of the complex $[Ru([9]aneS_3)(dipa)Cl]^+$ **6** presents the vibration pattern found in the literature[23,24] namely three sharp bands at 1527, 1581 and 1630 cm^{-1} and several peaks above 3100 cm^{-1}. The most energetic bands at 3364, 3271 and 3210 cm^{-1} can be assigned to amine stretching vibrations ($\nu_{N\text{-}H}$).[24] In the same region, free dipa has only one band at 3253 cm^{-1}. The NMR spectrum of **6** shows two distinct peaks for the NH proton (determined in water–D_2O (9:1)) δ at 9.63 and 9.48 (1H, s). However, in acetone, only one NH peak is present suggesting that the labile Cl is being replaced by H_2O.

The eleven aromatic resonances in the ^1H NMR spectrum of $[Ru([9]aneS_3)(tpy)Cl]^+$ **8** were assigned. The inequivalence of the aromatic protons for the tpy ligand suggests that tridentate binding is not occurring. Moreover the ES mass spectrum of this complex presented in Fig. S2 shows the characteristic pattern of a bidentate complex, with peaks corresponding to the M^+, $[M - 64]^+$ and $[M - 92]^+$ ions at *m*/*z* 550, 486 and 458 respectively. Although tpy behaves here as a bidentate ligand, it differs from the other bidentate ligands studied because it has an additional pyridyl group, which can interact with the other co-ordinating atoms, especially chlorine. The presence of two very abundant doubly charged ions of *m*/*z* 257.5 and 243.5 ($[M - Cl]^{2+}$ and $[M - Cl - CH_2CH_2]^{2+}$) which are not formed, at least with significant abundance, for the other bidentate complexes, and the mono-charged species of *m*/*z* 534 and 514 ($[M - Cl + F]^+$ and $[M - Cl - H]^+$), are an example of the predominance of Cl loss over other common fragmentation processes such as C–S cleavage. In addition, all the ions mentioned above are associated with loss of co-ordinated Cl. This points to increased tension in the Ru–Cl bond, induced by the non-co-ordinating pyridyl group, leading to a facile loss of Cl. However the co-ordination of smaller atoms such as F (arising from the PF_6^- counter ion) is possible, because the distance between the co-ordinated halogen and the pyridyl ring increases. Interestingly, if acetonitrile is used as a solvent in NMR a subset of peaks is observed indicating that it is replacing the Cl ligand. This is consistent with conclusions drawn from mass spectrometry where the free pyridyl ring of tpy destabilises the axial Cl atom allowing the formation of $[Ru([9]aneS_3)(tpy)]^{2+}$. The NMR and mass spectra results were found to be consistent with the crystal structure (see below), which indicates that tpy is in fact bound *via* two of the three nitrogens leaving one ring free.

The NMR spectrum of $[Ru([9]aneS_3)(bq)Cl]^+$ **9** is unique among the spectra of the complexes reported here since the protons of each of the CH_2 groups in the $[9]aneS_3$ macrocycle ligand have a distinct environment. There are six multiplets of eight peaks suggesting that there is C_2 symmetry and each proton is coupled to three others. The bulkiness of the bq ligand and its resulting distortion when bound (see X-ray) most probably gives rise to this inequivalence. The crystal structure shows that the ligand is deflected away from the S–S–Ru–N–N plane and twisted about the interannular C–C bond. The related ligand, dhmf, was used in an attempt to synthesize an analogous complex, however a mixture of the desired complex (70%) and the "free" ligand (30%) was always obtained. In the case of dhmf, due to the extra rigidity of the framework, twisting about this interannular C–C bond is not possible, and consequently, co-ordination is much more difficult.

The solid obtained from the synthesis of complex $[Ru([9]aneS_3)(dhmf)Cl]^+$ **14** has an ES mass spectrum showing peaks $[M - 64]^+$ and $[M - 92]^+$ characteristic of this family of complexes. Other ions formed by rearrangement of the polypyridyl moiety can also be observed. The unco-ordinated ligand in the solid is revealed in the mass spectrum by the presence of a peak with an unusually high relative abundance at *m*/*z* 311 corresponding to the protonated ligand. This fact does not imply an unreacted mixture since no precursor $[Ru([9]aneS_3)(dmso)Cl_2]$ was detected. This precursor is soluble in water and slightly soluble in several organic solvents and since the eluent used was a 50:50 water–methanol mixture the absence in the ES mass spectrum of **14** of the peak corresponding to the rapidly formed $[Ru([9]aneS_3)(dmso)(H_2O)Cl]^+$ species, obtained from $[Ru([9]aneS_3)(dmso)Cl_2]$, indicates that there is no contamination with the precursor.

Structural studies

Molecular structures of $Ru^{II}[9]aneS_3$ polypyridylic complex cations. The crystal structures of $[Ru([9]aneS_3)(dipa)Cl]PF_6$ **6**, $[Ru([9]aneS_3)(bpym)Cl]PF_6$ **7**, $[Ru([9]aneS_3)(tpy)Cl]PF_6$ **8**, $[Ru([9]aneS_3)(bq)Cl]PF_6{\cdot}CH_3CN$ **9**, $[Ru([9]aneS_3)(dip)Cl]BF_4$ **11** and $[Ru([9]aneS_3)(dppz)Cl]PF_6{\cdot}0.25H_2O$ **13** were determined by X-ray diffraction. The asymmetric unit of complex **6** contains a discrete cation $[Ru([9]aneS_3)(dipa)Cl]^+$ and a PF_6^- anion both with *m* crystallographic symmetry. The asymmetric unit of $[Ru([9]aneS_3)(bpym)Cl]PF_6$ **7** is composed of a $[Ru([9]aneS_3)(bpym)Cl]^+$ cation and a PF_6^- anion also with *m* crystallographic symmetry. The unit cell of **8** consists of $[Ru([9]aneS_3)(tpy)Cl]^+$ cations and PF_6^- anions. The unit cell of **9** is composed of four $[Ru([9]aneS_3)(bq)Cl]^+$ cations, four disordered PF_6^- anions and four CH_3CN solvent molecules. The unit cell of **11** contains discrete $[Ru([9]aneS_3)(dip)Cl]^+$ cations and BF_4^- anions. The crystal structure of **13** is built from an asymmetric unit composed of two complex $[Ru([9]aneS_3)(dppz)Cl]^+$ cations, two disordered PF_6^- anions and a water molecule with an occupancy of 0.25. Several crystals of **13** were investigated but all showed weak diffraction patterns. The *hkl* data of the selected crystal used for data collection had a high R_{int} value of 0.158 and a high final *R* value of 0.124. A detailed analysis of the structural features of the structure of **13** is therefore problematic. However, two crystallographically independent cations have structural parameters that bear enough accuracy for an unequivocal characterisation of the co-ordination environment of the ruthenium centre in both cases. The inclusion of this complex allows a much broader discussion of the structural trends in this family of complexes. Furthermore, the bond lengths and angles found for the two independent cations are identical within standard limits. In the present discussion the average values for these structural parameters will be used, unless otherwise stated.

For comparison purposes the structures of the six complexes cations will be discussed together while crystal packing will be discussed only at the end of this section. Molecular diagrams with the corresponding atomic notation scheme used are presented in Figs. 1, 2, 3, 4, 5 and 6 for complex cations **6**, **7**, **8**, **9**, **11** and **13**, respectively. Selected bond lengths and angles in the ruthenium co-ordination sphere are given in Table 1. In all structures the metal centre displays a distorted octahedral co-ordination sphere with the equatorial plane defined by two

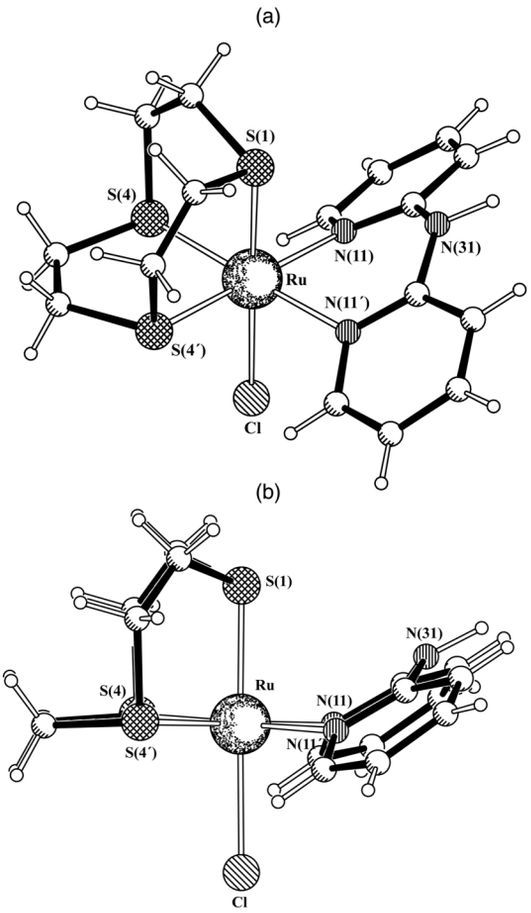

Fig. 1 Molecular structure of $[Ru([9]aneS_3)(dipa)Cl]^+$ **6**: (a) side view with the labelling scheme adopted; (b) view along the axis defined by the two nitrogen donor atoms of dipa showing the boat conformation of the six-membered chelate ring and the special orientation relative to the equatorial plane adopted by this ligand.

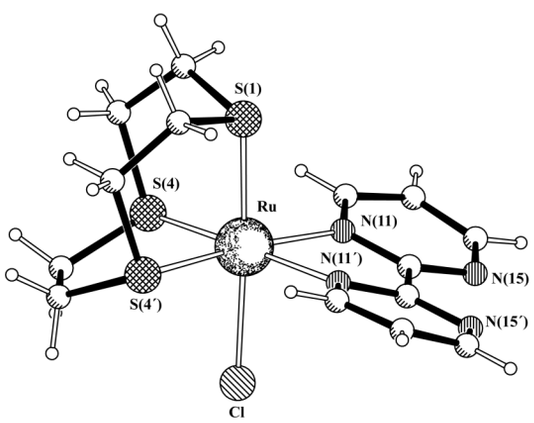

Fig. 2 Molecular structure of $[Ru([9]aneS_3)(bpym)Cl]^+$ **7** with the labelling scheme adopted.

macrocyclic sulfur donor atoms and two nitrogen atoms from the polypyridylic ligand: dipa **6**, bpym **7**, tpy **8**, bq **9**, dip **11** or dppz **13**. Six-co-ordination is completed *via* the remaining sulfur macrocyclic atom and a chlorine atom.

Table 2 lists the relevant structural parameters for the characterisation of the complexes together with the data for other closely related $Ru^{II}[9]aneS_3$ polypyridylic complexes. The crystal data include the complex cations $[Ru([9]aneS_3)(dpm)Cl]^+$ **4**, $[Ru([9]aneS_3)(dpk)Cl]^+$ **5**, $[Ru([9]aneS_3)(bpy)Cl]^+$ **15** and $[Ru([9]aneS_3)(phen)Cl]^+$ **16**. Complexes **15** and **16** have been reported in our previous study.[9b] Complexes **4** and **5** were also investigated by us using X-ray single crystal diffraction.[25]

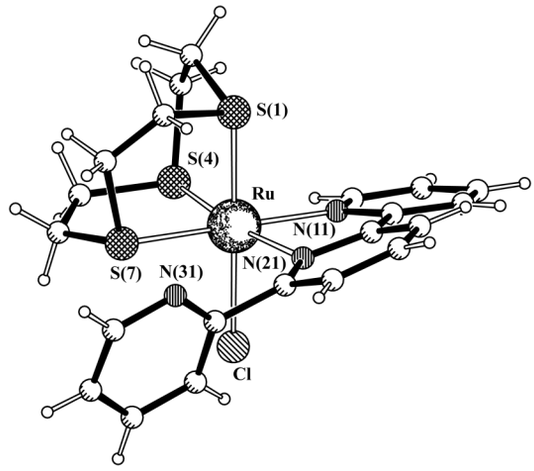

Fig. 3 Molecular structure of $[Ru([9]aneS_3)(tpy)Cl]^+$ **8** with the labelling scheme adopted.

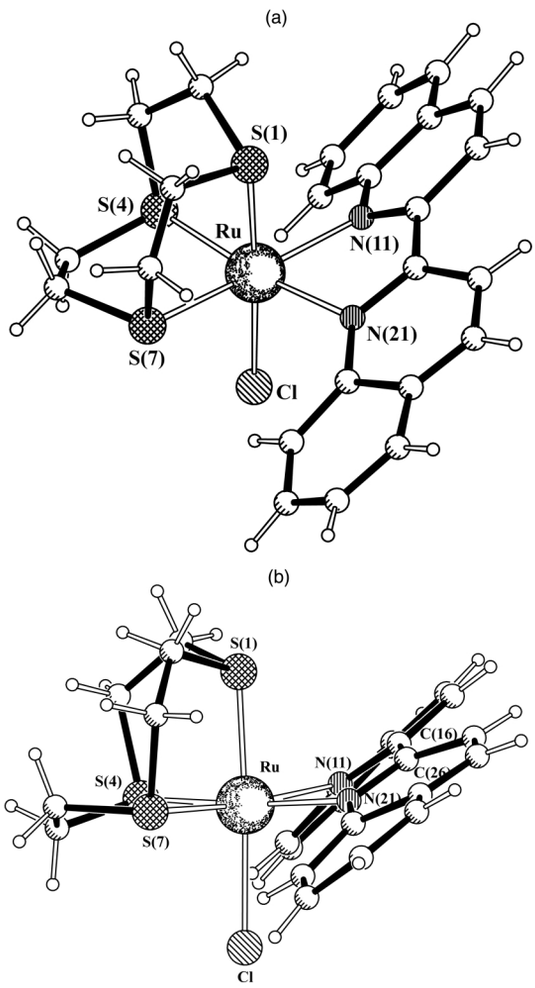

Fig. 4 Molecular structure of $[Ru([9]aneS_3)(bq)Cl]^+$ **9**: (a) side view with the labelling scheme adopted; (b) view along the axis defined by the two nitrogen donor atoms of bq showing the special orientation relative to the equatorial co-ordination plane adopted by this ligand.

Unfortunately both compounds were composed of *ca.* 50% crystal and 50% powder and gave very poor diffraction patterns. However in both cases it was possible to locate unambiguously all non-hydrogen atoms and to refine the positions of the sulfur and ruthenium atoms with anisotropic thermal parameters and the remaining non-hydrogen atoms with isotropic thermal parameters. The final quality of the crystal structures of these two compounds is not good, but

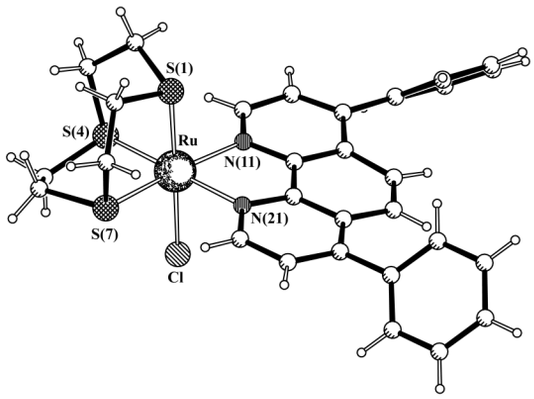

Fig. 5 Molecular structure of $[Ru([9]aneS_3)(dip)Cl]^+$ **11** with the labelling scheme adopted.

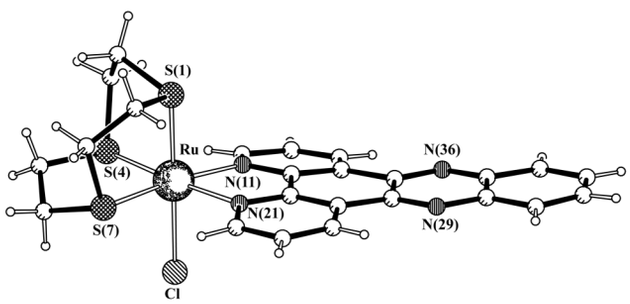

Fig. 6 Molecular structure of one of the independent $[Ru([9]aneS_3)(dppz)Cl]^+$ **13** cations, with the labelling scheme adopted. The $[9]aneS_3$ ligand has a type III conformation.

the dimensions involving the ruthenium centre in both cases are sufficiently accurate to be included in a wider discussion of some structural features associated with polypyridyl $Ru^{II}[9]aneS_3$ complexes. Complexes **4**, **5**, **15** and **16** have *fac*-octahedral geometry with the polypyridyl ligand in the equatorial co-ordination plane, an arrangement similar to that seen for the new crystal structures reported here. The terpyridyl ligand has three possible nitrogen donor atoms, allowing tridentate co-ordination. This is undoubtedly the preferred mode of tpy when the metal centre has three *mer* co-ordination positions available and has been found for the majority of ruthenium complexes containing tpy.[26] However, there are several examples of ruthenium complexes with tpy behaving as a bidentate ligand,[27] as occurs in **8**, in which the facial co-ordination of $[9]aneS_3$ prevents co-ordination of the third nitrogen donor atom N(31). The assignment of the nitrogen N(31) and the carbon C(33) atoms is unambiguous (see Experimental section). In the crystal structure of **8** this nitrogen is 4.400(6) Å from the *mer* position occupied by the sulfur macrocyclic S(7) atom (see Fig. 3) but only 0.224(6) Å out of the equatorial co-ordination plane, which makes an angle of 73.2(2)° with the pyridyl ring 3 (rings are numbered according to the nitrogen atom they contain). The orientation of this ring suggests that N(31) can easily replace S(7) in the metal co-ordination sphere. However the thermodynamic stability gained through the macrocycle effect from the co-ordination of the three sulfur donor atoms of $[9]aneS_3$ favours the isomer found by X-ray diffraction analysis. A structure such as $[Ru([9]aneS_3)(tpy)]^{2+}$, resulting from replacement of the axial Cl by the nitrogen N(31) of ring 3 in the metal co-ordination sphere, is impossible because tpy cannot be *fac* while $[9]aneS_3$ is not *mer*. In complex **8** the bpy unit formed by pyridyl rings 1 and 2 is twisted around the interannular C–C bond with a dihedral angle between the two rings of 16.6(3)°. However the major twisting of 56.3(2)° involves the co-ordinated ring 2 and the non-co-ordinated ring 3. These values are within the range expected for metal complexes in which the tpy adopts a chelating bidentate behaviour.[27]

In complex **9** the bq ligand also exhibits a twist of 16.5(10)° around the interannular C–C bond, possibly in order to minimise steric interactions between the side rings of this ligand and the macrocyclic sulfur atoms S(7) and S(4) (see below and Fig. 4b). By contrast, in complex **15**, the bpy ligand is nearly planar with the twist angle between rings 1 and 2 reduced to 1.4°. Complex **7** has C_s symmetry and as a consequence the bpym ligand is perfectly planar with a twist angle of 0°.

Complexes **6** and **9** show a pronounced tilt of the polypyridylic ligand (dipa or bq) relative to the equatorial co-ordination plane. This tilting is clearly seen in Figs. 1(b) and 4(b), which show the molecular structures of the complex cations **6** and **9** projected along the axis defined by the two nitrogen polypyridylic donor atoms, and can be characterised by the angle *a*, which is defined as the dihedral angle between the equatorial plane (*e.g.* atoms S(4), S(7), N(11) and N(21) in **9**) and the plane of the four pyridyl atoms participating in the chelate ring (*e.g.* N(11), C(16), C(26), N(21) in **9**). This angle takes values of 32.7(3) and 31.3(7)°, for **6** and **9** respectively. Complex **5** with dpk has a similar tilt with an *a* angle of 33.4(16)°, which is reduced in **4** with dpm to 22.3(6)° (average value). By contrast, complexes **11**, **13**, **15** and **16** (values quoted in Table 2) show much smaller *a* angles indicating that the polypyridyl ligands are almost in the equatorial co-ordination plane. An intermediate situation occurs for **7** and **8**, in which the polypyridyl ligand (bpym or tpy) exhibits *a* angles of 17.2(2) and 13.4(3)° respectively. However, the value of the tilt angle presented by the bpym ligand in complex **7** is unexpectedly high when compared to that found for bpy in **15**, which is close to 0°.

This comparison shows that increasing the lateral length of the polypyridyl ligand either by introducing a bridging group between the two pyridyl rings (CH_2 in dpm, C=O in dpk or NH in dipa) or by expanding the aromatic system of bpy, by adding two fused rings to give the bq ligand, has a dramatic effect on the overall geometry of the complex. By contrast increasing the bulk at the back of the phen skeleton by introducing two phenyl groups (dip) or expanding the aromatic system adding two fused rings (dppz) has negligible influence. Rotation of the dipa or bq ligand around the axis defined by the nitrogen donor atoms towards the equatorial co-ordination plane leads to two short close contacts (*ca.* 1.80 and 1.74 Å in **9** and 2.42 and 2.37 Å in **6**) between the equatorial sulfur atoms and the hydrogen atoms of the polypyridyl ring closest to the ruthenium(II) first co-ordination sphere. This increases considerably the steric strain in the metal complex.

In complex **6** the dipa ligand adopts a boat configuration on chelation to the metal with a dihedral angle between pyridyl rings 1 and 2 of 32.2(1)°. The sp^3 bridging nitrogen is 0.264(8) Å and the ruthenium atom is 0.831(9) Å above the plane defined by the pyridyl atoms participating in the six-membered chelate ring. The bond angle centred at the bridging nitrogen C(16)–N(31)–C(16′) is 127.4(7)°. The lengths of the bridge bonds N–C [1.409(6) Å] are longer than those found for C–N bonds within the pyridyl rings [1.328(7) and 1.356(7) Å]. These structural results indicate the absence of cross-conjugation effects between the two pyridyl rings *via* the bridging nitrogen atom.

All complexes quoted in Table 2 contain comparable Ru–S and Ru–N bond lengths in the ruthenium(II) co-ordination sphere. In all cases, except **4**, the Ru–S axial bonds are slightly shorter than the equatorial Ru–S bonds due to the differential *trans* influence of the chloride and the polypyridyl ligands. Complexes **7**–**9**, **11**, **13**, **15** and **16** have similar N–Ru–N values, within the range 75.2(6) to 79.1(2)°, which reflects the small bite angles of the bpym, tpy, bq, dip, dppz, bpy and phen polypyridyl ligands. When this steric constraint is reduced wider N–Ru–N angles close to the ideal octahedral value of 90° as expected. Thus complexes of dpm **4**, dpk **5** and dipa **6** exhibit

Table 1 Selected bond lengths and angles for complexes **6**–**9**, **11** and **13**

6	[Ru([9]ansS_3)(dipa)Cl]$^+$			
	Ru–N(11)	2.116(5)	Ru–Cl	2.450(3)
	Ru–S(1)	2.285(3)	Ru–S(4)	2.307(2)
	N(31)–C(16)	1.409(6)	C(16)–N(11)	1.328(7)
	N(31)–H(31)	0.861(11)	C(12)–N(11)	1.356(7)
	N(11′)[a]–Ru–N(11)	84.9(2)	N(11)–Ru–S(4′)[a]	178.6(1)
	S(4′)[a]–Ru–S(4)	87.3(1)	S(1)–Ru–Cl	179.0(1)
	C(16′)[a]–N(31)–C(16)	127.4(7)	C(16′)[a]–N(31)–H(31)	113.3(12)
7	[Ru([9]ansS_3)(bpym)Cl]$^+$			
	Ru–N(11)	2.112(4)	Ru–Cl	2.452(2)
	Ru–S(1)	2.294(3)	Ru–S(4)	2.303(2)
	N(11)–Ru–N(11′)[b]	77.9(2)	N(11′)[b]–Ru–S(4)	174.4(1)
	S(4)–Ru–S(4′)[b]	86.6(1)	S(1)–Ru–Cl	177.0(1)
8	[Ru([9]ansS_3)(tpy)Cl]$^+$			
	Ru–N(11)	2.092(4)	Ru–N(21)	2.152(4)
	Ru–S(7)	2.327(2)	Ru–Cl	2.434(2)
	Ru–S(1)	2.280(2)	Ru–S(4)	2.297(2)
	N(11)–Ru–N(21)	78.0(2)	N(11)–Ru–S(7)	178.2(1)
	N(21)–Ru–S(4)	172.1(1)	S(4)–Ru–S(7)	86.9(1)
	S(1)–Ru–Cl	179.0(1)		
9	[Ru([9]aneS_3)(bq)Cl]$^+$			
	Ru–N(11)	2.159(15)	Ru–N(21)	2.171(14)
	Ru–S(1)	2.287(5)	Ru–S(7)	2.320(6)
	Ru–S(4)	2.329(6)	Ru–Cl	2.451(5)
	N(11)–Ru–N(21)	75.2(6)	N(11)–Ru–S(7)	171.4(4)
	N(21)–Ru–S(4)	173.2(4)	S(7)–Ru–S(4)	85.8(2)
	S(1)–Ru–Cl	176.9(2)		
11	[Ru([9]aneS_3)(dip)Cl]$^+$			
	Ru–N(11)	2.098(5)	Ru–N(21)	2.104(6)
	Ru–S(1)	2.274(3)	Ru–S(7)	2.301(3)
	Ru–S(4)	2.307(3)	Ru–Cl	2.417(4)
	N(11)–Ru–N(21)	79.1(2)	N(11)–Ru–S(7)	175.1(2)
	N(21)–Ru–S(4)	175.1(2)	S(7)–Ru–S(4)	87.7(1)
	S(1)–Ru–Cl	177.6(1)		
13	[Ru([9]aneS_3)(dppz)Cl]$^+$[c]			
	Ru–N(11)	2.110(11), *2.108(12)*	Ru–N(21)	2.104(11), *2.081(11)*
	Ru–S(1)	2.289(5), *2.290(5)*	Ru–S(4)	2.314(4), *2.305(4)*
	Ru–S(7)	2.296(5), *2.298(5)*	Ru–Cl	2.429(5), *2.433(5)*
	N(11)–Ru–N(21)	78.3(4), *78.5(5)*	N(11)–Ru–S(7)	173.5(3), *175.5(4)*
	N(21)–Ru–S(4)	175.2(3), *175.5(4)*	S(7)–Ru–S(4)	87.6(2), *87.4(2)*
	S(1)–Ru–Cl	179.0(2), *176.5(2)*		

Symmetry transformations used to generate equivalent atoms: [a] $x, y, \frac{1}{2} - z$; [b] $x, -y + \frac{1}{2}, z$. [c] The italicised values correspond to the second molecule present in the asymmetric unit.

angles of 86.2(4) (average value), 85.5(14) and 84.9(2)° respectively.

The S–C–C–S, C–S–C–C and C–C–S–C endocyclic torsion angles, given Table S1, indicate, in the solid state, four different conformations adopted by the macrocycle for complexes **6**–**9**, **11**, **13** and **15**, **16**. The root mean square deviations (r.m.s.) of the atomic positions, excluding the hydrogen atoms, calculated for the conformations of [9]aneS_3 in these metal complexes have also been deposited as Table S2. In **6** and **7** the macrocycle displays two different conformations, both with C_s symmetry. Complex **6** has a type I conformation while **7** exhibits a type II conformation. The r.m.s. deviation between these two conformations is large at 0.267 Å. In both complexes two SCH_2-CH_2SCH_2 moieties of the macrocyclic backbone are related by a crystallographic mirror plane, perpendicular to the equatorial co-ordination plane, containing the axial donor atoms. Complexes **9**, **11**, **15** and **16** display a type III conformation. The r.m.s. deviations (between 0.032 and 0.070 Å) for the alignment of the [9]aneS_3 macrocyclic backbone of these complexes, shows that the macrocycle adopts the same conformation in all cases. Complex **13** exhibits two slightly different conformations with one of the independent molecules present in the asymmetric unit unequivocally adopting a type III conformation and the other an intermediate conformation between types I and III. The fitting of the two independent conformations of **13** gives a r.m.s. of 0.185 Å. Furthermore the alignment of the intermediate conformer of **13** with the type III conformation of **9**, **11**, **15** and **16** leads to r.m.s. deviations ranging from 0.177 to 0.119 Å. When this intermediate conformer is fitted with the type I conformer of **6** a smaller r.m.s. deviation of 0.082 Å is obtained. Finally the [9]aneS_3 ligand in complex **8** has a conformation similar to the intermediate conformer found for **13**. The alignment of the macrocycle backbone of **8** with the intermediate conformer of **13** and with the type I conformer of **6** give r.m.s. values of 0.069 and 0.123 Å respectively. The fitting of the [9]aneS_3 ligand of **8** with the type III conformer of **9** also

Table 2 Comparison of dimensions (distances in Å, angles in °) in the crystal structures of Ru^{II}/[9]ansS_3 polypyridylic complexes

Complex	⟨Ru–S_{eq}⟩	Ru–S_{ax}	Ru–Cl	⟨Ru–N⟩	N–Ru–N	*a*
4 [Ru([9]aneS_3)(dpm)Cl]$^{+}$ [a,b]	2.293(6)	2.312(7)	2.444(6)	2.126(18)	85.0(7)	24.7(5)
	2.289(7)	*2.238(9)*	*2.447(8)*	*2.140(20)*	*87.3(8)*	*19.9(6)*
5 [Ru([9]aneS_3)(dpk)Cl]$^{+}$ [b]	2.333(4)	2.283(10)	2.478(11)	2.097(3)	85.5(14)	33.4(16)
6 [Ru([9]aneS_3)(dipa)Cl]$^{+}$	2.307(2)	2.285(3)	2.450(3)	2.116(5)	84.9(2)	32.7(3)
7 [Ru([9]aneS_3)(bpym)Cl]$^{+}$	2.303(2)	2.294(3)	2.452(2)	2.112(4)	77.9(2)	17.2(2)
8 [Ru([9]aneS_3)(tpy)Cl]$^{+}$	2.312(2)	2.280(2)	2.434(2)	2.122(4)	78.0(2)	13.4(3)
9 [Ru([9]aneS_3)(bq)Cl]$^{+}$	2.324(5)	2.287(5)	2.451(5)	2.165(14)	75.2(6)	31.3(7)
11 [Ru([9]aneS_3)(dip)Cl]$^{+}$	2.304(3)	2.274(3)	2.417(4)	2.101(5)	79.1(2)	6.6(1)
13 [Ru([9]aneS_3)(dppz)Cl]$^{+}$ [a]	2.305(4)	2.289(5)	2.429(5)	2.107(11)	78.3(4)	3.3(6)
	2.302(4)	*2.290(5)*	*2.433(5)*	*2.094(11)*	*78.5(5)*	*7.2(9)*
15 [Ru([9]aneS_3)(bpy)Cl]$^{+}$ [c]	2.318(2)	2.287(2)	2.476(2)	2.106(6)	78.0(2)	3.0
16 [Ru([9]aneS_3)(phen)Cl]$^{+}$ [c]	2.288(2)	2.272(2)	2.438(2)	2.089(5)	78.8(2)	6.2

[a] The italicised values are for the second molecule present in the asymmetric unit. [b] Ref. 25. [c] Ref. 9(*a*).

gives a small r.m.s. deviation of 0.080 Å. This latter conformation has been found for many metal transition complexes where the macrocycle adopts a facial co-ordination mode.[22] The free macrocycle also exhibits a type III conformation in the solid state.[28] A molecular mechanics and dynamics study, in the gas phase, gave thirteen conformations with energies between 4.5 and 8.3 kcal mol^{-1}, the conformation with the lowest energy was of type III.[29] Among the remaining twelve conformations none were of type I or II, presumably because conformational preference changes on chelation.

Crystal structures

The crystal structures of complexes **6**–**9**, **11** and **13** can be analysed in an effort to understand the factors that govern crystal packing, which may play a significant role in the different [9]aneS_3 conformations found in the solid state in this study (see above). All of the complexes exhibit intermolecular interactions resulting from C–$H^{\delta+}\cdots F^{\delta-}$ hydrogen bonds between fluorine atoms of the anions (PF_6^- or BF_4^-) and hydrogen atoms of the macrocycle framework or/and polypyridyl ligands. In addition, the crystal structures of complexes **6**, **7** and **8** are stabilised by hydrogen bonding interactions between the unco-ordinated nitrogen and chlorine atoms. The dimensions of the hydrogen bonds found for **6**–**8** and **11** are given in Table S3. Possible hydrogen bonds for **9** and **13** are not included since their PF_6^- anions are disordered over two positions in the crystal lattice with similar statistical significance, preventing detailed analysis. Nevertheless, it is clear from the intermolecular C–H···F distances found for both complexes that these types of interactions are present in the crystal structures.

The molecular assembly of [Ru([9]aneS_3(dip)Cl]$^{+}$ cations and BF_4^- anions in complex **11** results in one of the most interesting solid state structures. The BF_4^- anions are aggregated in layers and when viewed along the *a* crystallographic axis, as shown in Fig. 7(a), the stacking of these layers results in the formation of open channels running through the crystal structure. Each one of the larger channels, composed of six chains of BF_4^- anions, accommodates one chain of [Ru([9]aneS_3)(dip)Cl]$^{+}$ cations exhibiting a twofold screw axis symmetry, imposed crystallographically. Within each chain the dip aromatic ligands adopt an almost co-facial π stacking with an inter-planar distance between two adjacent parallel aromatic rings of 3.75 Å (see Fig. 7b). The [Ru([9]aneS_3)(dip)Cl]$^{+}$ chains are connected by BF_4^- bridges *via* short charge assisted intermolecular C–$H^{\delta+}\cdots F^{\delta-}$ contacts. One side of these bridges involves two hydrogens from two different CH_2 groups of the macrocycle ligand and one fluorine atom of the BF_4^- in a bifurcated geometric arrangement (C–$H^{\delta+}\cdots F^{\delta-}$distances of 2.45 and 2.53 Å). The other side is comprised of a second fluorine atom of the BF_4^- anion and an hydrogen from the polypyridyl ligand of a second complex cation, in a linear arrangement (C–$H^{\delta+}\cdots F^{\delta-}$ of 2.45 Å). From the point of view of hydrogen bonding interactions this compound exhibits a two-dimensional polymeric structure.

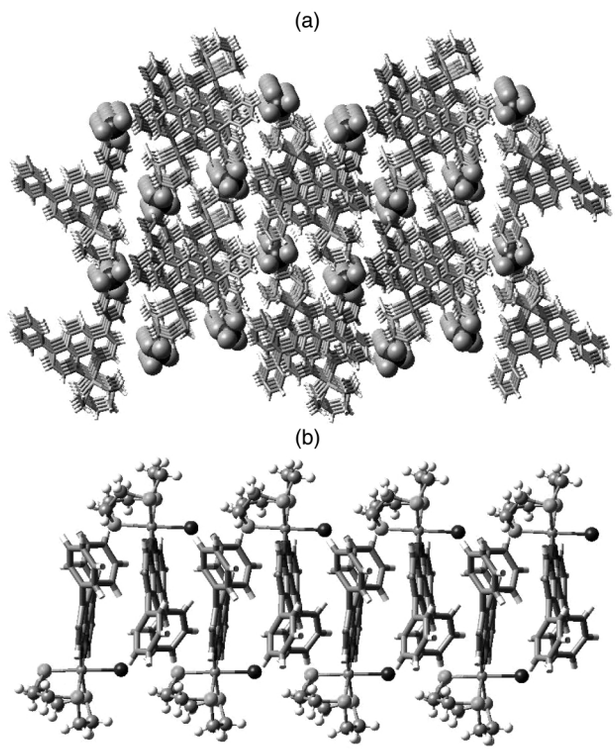

Fig. 7 Crystal-packing diagram of [Ru([9]aneS_3)(dip)Cl]BF_4 **11**: (a) view along the *a* crystallographic axis showing that the large open channels of BF_4^- anions accommodating a helicoidal chain of [Ru([9]aneS_3)(dip)Cl]$^{+}$ cations; (b) view showing the π stacking arrangement of the cations in the chain.

The crystal-packing of complex **6** reveals that chains of [Ru([9]aneS_3)(dipa)Cl]$^{+}$ cations are assembled in layers separated by layers of PF_6^- anions. Within these layers the cations are linked *via* hydrogen bonds between the free nitrogen atom of dipa ligands and Cl atoms (two N–$H^{\delta+}\cdots Cl^{\delta-}$-distances of 2.18(11) Å). These chains, related by the crystallographic inversion centre, are subsequently connected by PF_6^- bridges *via* short charged assisted C–$H^{\delta+}\cdots F^{\delta-}$ intermolecular contacts involving a fluorine atom and the dipa ligands (two C–$H^{\delta+}\cdots F^{\delta-}$ distances of 2.54 Å). When the crystal packing is viewed along the *b* crystallographic axis the C–$H^{\delta+}\cdots F^{\delta-}$ and N–$H^{\delta+}\cdots Cl^{\delta-}$ intermolecular interactions give rise to a two-dimensional superstructure containing larger rings formed by four complex units from adjacent chains of cations and two PF_6^- anions as shown in Fig. S3.

The assembly of [Ru([9]aneS_3)(bpym)Cl]$^{+}$ cations and PF_6^- anions in complex **7** results in π stacking of the bpym rings along the *b* axis in a co-facial arrangement, with a minimum inter-planar distance between two adjacent aromatic rings of 3.42 Å, related by a crystallographic inversion centre.

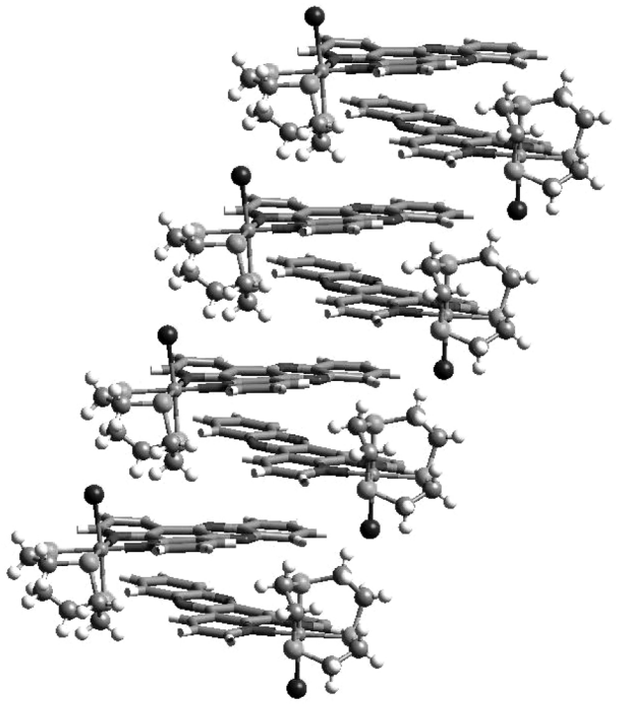

Fig. 8 The π stacking arrangement of the $[Ru([9]aneS_3)(dppz)Cl]^+$ cations in the crystal structure of complex **13**.

Fig. S4 presents the structural motif derived from an hydrogen bond analysis where two complex cations are connected *via* $C–H^{\delta+}\cdots Cl^{\delta-}$ intermolecular interactions (two $C–H^{\delta+}\cdots Cl^{\delta-}$ distances of 2.80 Å) between the bpym ligand and chlorine atoms to form a large centrosymmetric ring. This dimeric fragment then interacts concomitantly with neighbouring dimers *via* $C–H^{\delta+}\cdots N^{\delta-}$ hydrogen bonds involving the two free nitrogen atoms of bpym and two adjacent CH_2 groups of the macrocycle framework forming a three-dimensional network (two $C–H^{\delta+}\cdots N^{\delta-}$ distances of 2.48 Å). The inclusion of PF_6^- anions in the crystal results in the stabilisation of these networks by $C–H^{\delta+}\cdots F^{\delta-}$ hydrogen bonds ($C–H^{\delta+}\cdots F^{\delta-}$ bifurcated bonds with two distances of 2.44 Å and two linear $C–H^{\delta+}\cdots F^{\delta-}$ bonds with distances of 2.40 Å).

In complex **9** zigzag chains of $[Ru([9]aneS_3)(bq)Cl]^+$ cations are intercalated by other zigzag chains of PF_6^- anions, but the packing shows no special features.

The molecular assembly of the complex cations and anions in complexes **8** and **13** shows no special aspects except for the fact that in **8** some hydrogen atoms of the macrocycle and of the polypyridyl ligands are directed towards the PF_6^- anions and $C–H^{\delta+}\cdots F^{\delta-}$ hydrogen bonds occur. In addition, the crystal structure is stabilised *via* short charged assisted $C–H^{\delta+}\cdots N^{\delta-}$ and $C–H^{\delta+}\cdots Cl^{\delta-}$ intermolecular contacts between the free nitrogen atom of the tpy ligand and the macrocycle, and the chlorine atom of neighbouring cations. This set of weak intermolecular contacts also leads to the formation of a three-dimensional network of PF_6^- anions and $[Ru([9]aneS_3)(tpy)Cl]^+$ cations in the crystal.

In the crystal structure of complex **13** two chains of $[Ru([9]aneS_3)(dppz)Cl]^+$ cations, formed by the independent crystallographic molecules (the asymmetric unit contains two independent cations), are in a π-stacking geometric arrangement, as shown in Fig. 8. Within these chains the cations are related by a twofold crystallographic screw axis. The independent neighbour cations are rotated with respect to each other by *ca.* 51.6° (the dihedral angle between planes perpendicular to the dppz ligands containing the axial donor atoms) with a minimum inter-planar distance of 3.35 Å. In **13** as well as in **11** the inter-planar distance found may simply represent the minimum van der Waals approach between the two larger π rings of dppz or dip. Thus the inter-planar distance between two dip rings is larger than that involving two dppz rings due to the presence of two bulky phenyl groups in its aromatic skeleton. Furthermore, the packing geometry of the cations for these two complexes represents the minimisation of the steric interaction within their crystal structures.

Conclusion

Novel $[Ru^{II}([9]aneS_3)(L)Cl]^+$ complexes containing bidentate polypyridyl ligands or monodentate ligands were synthesized in a single step from the starting compound $[Ru([9]aneS_3)(dmso)Cl]^+$. The synthetic pathway was achieved under mild conditions to produce complexes containing polypyridyl ligands with very different molecular architectures such as dppz, dhmf, dip or pdi. In **2** and **3** the diamine ligands (pda or dap) undergo Ru assisted oxidation, *in situ*, to the corresponding imine forms (pdi or phi). Strikingly, in **5**, the C=O bridge of dpk ligand retains double bond character in spite of the synthesis being carried out in a nucleophilic solvent. All eight complexes characterised by X-ray diffraction exhibit a distorted octahedral geometric arrangement with the $[9]aneS_3$ co-ordinated facially to the Ru^{II}. In the case of tpy, the co-ordination mode of the crown ether prevents the third potential nitrogen atom of the tpy ligand from binding. Thus in the complex $[Ru([9]aneS_3)(tpy)Cl]^+$ the tpy ligand adopts bidentate behaviour analogous to that found for all the complexes reported here. An increase in the lateral length of the polypyridyl ligand, by adding a bridging group between two pyridyl rings or by expanding the aromatic system by introducing two fused rings, has a drastic effect on the overall geometry of the complex leading to a pronounced tilt of the polypyridyl ligand relatively to the N_2S_2 equatorial co-ordination plane. By contrast an increase in bulk at the back of the phenanthroline skeleton, through the introduction of phenyl groups or the expansion of the aromatic system by adding two fused rings, has a negligible effect.

The crystal structures were found to be largely stabilised by hydrogen bond interactions and the extended aromatic systems, with recognised intercalative properties such as dppz and dip, exhibit π stacking arrangements which mimic the structure of polypyridyl complexes intercalated with DNA.

Experimental

Physical measurements

All NMR spectra were recorded on either a Bruker AMX spectrometer operating at 300 MHz or a Bruker ARX spectrometer operating at 400 MHz. The ^1H spectra were obtained using 16k data points and a sweep width of 14.04 ppm. dmso-*d*6 complexes (**1**, **12**), D_2O–water 1 : 9 (**2**, **6**), CD_3CN (**3**–**5**, **7**, **9**, **10** and **14**) and CD_3OD (**8** and **13**) were used as solvents with chemical shifts being referenced to dmso (δ 2.50), HOD (δ 4.75), CD_2HCN (δ 1.94) and CD_2HOD (δ 3.35), respectively. ^{13}C spectra were recorded using a sweep width of 250 ppm with 32k data points. Full proton decoupling was used. External 1,4-dioxane (δ 66.5) was used as a chemical shift reference. The UV/Vis spectra were obtained at room temperature on a JASCO V-560 spectrophotometer in dmso (**1**), water (**2**), CH_3CN (**3**–**10** and **14**) or 0.01 M phosphate buffer solution (**12**, **13**), IR spectra as KBr discs using a FTIR Mattson-7000 infrared spectrophotometer with 2 cm^{-1} resolution. Elemental analyses were obtained with a Carlo-Erba CHN or a LECO CHNS-932 Elemental Analyser.

With the exception of complexes **2** and **8**, the mass spectra were acquired with a VG AutoSpec (VG Analytical Manchester, UK) working in an EBE geometry mode. The instrument was equipped with a VG electrospray source and a Phoenix 20CU syringe pump (Fisons Instruments). The accelerating voltage applied was 4 kV. The spectra were

obtained at a scan rate of 8 s decade^{-1}. The mass spectrometer was operated at a nominal mass resolution of 1000 (10% valley). Methanol–water (50 : 50) was employed as the eluent. The monodentate complex **1** was dissolved in dmso prior to injection. The mass spectra of **2** and **8** were obtained using a VG ZAB-T four-sector instrument (VG Analytical Manchester, UK), which consisted of two high-mass, double focusing mass spectrometers of an overall BEBE design. The instrument was equipped with a VG electrospray source and a Harvard model 22 syringe pump. The acceleration voltage was 8 kV. The mass spectrometer was operated at a nominal mass resolution of 3000 (10% valley). A mixture of CH_3CN–water–acetic acid (50 : 49 : 1) was used as the eluent.

Synthesis

$RuCl_3$ hydrate (Johnson Matthey), the macrocycle polythioether [9]aneS_3, and the polypyridyls or related ligands pda, dap, ind, dpk, dipa, tpy, bq, 5-phen, dhmf (Sigma-Aldrich) and bpym (Lancaster) were used without further purification. The diimine ligands pdi and phi were obtained *in situ* from the Ru assisted oxidation of the complexes in the diamine form (pda and dap, respectively).[6b,18c,e] The ligands 5,6-dione,[30,31] dppz[11a] and dpm[32] were synthesized according to published methods, with slight experimental modifications.

Ruthenium(II) polypyridylic complexes. The synthesis of the starting material, *cis*-[Ru(dmso)$_4$Cl$_2$], was carried out with slight modifications to the method of Evans *et al.*[33] The synthesis of the precursor [Ru^{II}([9]aneS_3)(dmso)Cl$_2$], in the anhydrous form, was optimised by adapting the method of Landgrafe and Sheldrick.[34]

General method. The precursor [Ru^{II}([9]aneS_3)(dmso)Cl$_2$] (0.5 mmol) and a slight excess (<10%) of the polypyridyl ligand were mixed in 15–20 ml of deareated ethanol under an argon atmosphere and refluxed at 80–95 °C during 4–12 hours. The complexes were precipitated by adding NH_4PF_6, kept at −20 °C overnight, filtered off, washed with ethanol and diethyl ether and dried at 65 °C. Re-dissolution of the complexes in the minimum volume of acetonitrile and slow recrystallisation under a diethyl ether atmosphere afforded suitable crystals for X-ray diffraction studies.

Variations. (*i*) A large excess (≈100%) of polypyridyl ligand was used in preparation of ind **1**, pdi **2** and dhmf **14** complexes. (*ii*) 40–50 ml of deaerated EtOH were used for ind **1**, dpk **5**, dipa **6**, tpy **8**, bq **9**, dppz **13** and dhmf **14** complexes. (*iii*) Aqueous ethanol was used for the pdi and bpym complexes. The phi **3** complex was obtained after addition of 250 ml of water to the reaction mixture. (*iv*) The phi **3** complex was afforded after oxidation for 24 hours in air. (*v*) The pdi **2** and 5,6-dione **12** complexes were isolated as Cl^- salts while the dip **11** complex was obtained as the BF_4^- salt. The ind complex **1** is a neutral species. (*vi*) Single crystals of **1** and **11** were obtained from saturated ethanolic solutions standing at room temperature. The crystals of **8** and **13** were obtained from methanol and CH_3CN–acetone (1 : 1) solutions respectively.

Full experimental details of the preparation and characterisation of each compound are given in the ESI supplementary material.

Crystallography

The pertinent crystal data and refinement details are listed in Table S4 for complexes **6**–**9**, **11**, **13**. The X-ray data for these complexes as well as for **4** and **5** were collected at room temperature on a MAR research plate system using graphite Mo-Kα radiation at Reading University (UK). The crystals were positioned at 70 mm from the image plate and 95 frames were measured at 2° intervals using a counting time between 2 and 10 min adequate for the crystal under study. Data analysis was carried out with the XDS program.[35] Intensities were not corrected for absorption effects.

The structures were solved by a combination of direct methods, Fourier-difference syntheses and subsequent full-matrix least-squares refinements on F^2. All hydrogen atoms were introduced into the refinement at their ideal geometric positions, except for the hydrogen of the bridging nitrogen of the dipa in **6**, which was located from the difference map. The chemical identity of N(31) and C(33) in complex **8** was investigated carefully by replacing, in the refinement, carbon by nitrogen and *vice versa*. The crystal structure presented corresponds to the formulation with low R and R_w values.

All non-hydrogen atoms were refined with anisotropic thermal parameters. The fluorine atoms of the PF_6^- anions in complexes **9** and **13**, which exhibited positional disorder, were introduced in the refinement process using a disorder model comprising of two alternative positions with refined occupancies for each fluorine and using isotropic group thermal parameters. Refined occupancies for major components of disorder of 0.57(3) in **9** and 0.54(2) and 0.56(2) for two independent PF_6^- anions in **13** were obtained. The hydrogen atoms were refined with isotropic thermal parameters equal to 1.2 times that of the parent atom. The oxygen atom of the solvent water molecule was also refined with an isotropic thermal parameter. The occupation factor of oxygen was set to 0.25 in order to give a reasonable value for the thermal parameter. The hydrogen atoms of the water molecule were not introduced in the refinement process.

All calculations required to solve and refine the structures were carried out with SHELXS and SHELXL within the SHELX 97 package.[36] Molecular diagrams and the analysis of hydrogen bonds were performed with the PLATON[37a] and CERIUS 2[37b] graphical interfaces.

CCDC reference number 186/2203.

See http://www.rsc.org/suppdata/dt/b0/b004752j/ for crystallographic files in .cif format.

Acknowledgements

The authors acknowledge the financial support of Fundação para a Ciência e Tecnologia (FCT) and PRAXIS XXI (PRAXIS/PCEX/C/QUI/122/96). J. M. acknowledges a PhD grant from the FCT. We thank EPSRC (UK) and the University of Reading (UK) for funds for the Image Plate System and Mr A. W. Johans for his assistance with the crystallography.

References

1 A. M. Pyle and J. K. Barton, in *Progress in Inorganic Chemistry: Bioinorganic Chemistry*, ed. Stephen J. Lippard, John Wiley and Sons, London, 1990, vol. 38, p. 413; W. I. Sundquist and S. J. Lippard, *Coord. Chem. Rev.*, 1990, **100**, 293; B. Nordén, P. Lincoln, B. Åkerman and E. Tuite, in *Metal Ions in Biological Systems*, eds. A. Sigel and H. Siegel, Marcel Dekker, New York, 1996, vol. 23, ch. 7; C. S. Chow and F. M. Bogdan, *Chem. Rev.*, 1997, **97**, 1489; K. E. Erkkila, D. T. Odom and J. K. Barton, *Chem. Rev.*, 1999, **99**, 2777.
2 M. J. Clarke, F. Zhu and D. R. Frasca, *Chem. Rev.*, 1999, **99**, 2511.
3 J. K. Barton and E. Lolis, *J. Am. Chem. Soc.*, 1985, **107**, 708.
4 C. Orvig and M. J. Abrams, *Chem. Rev.*, 1999, **99**, 2201.
5 T. Meade, *Coord. Chem. Rev.*, 1999, **184**, 1.
6 (*a*) A. H. Krotz, L. Y. Kuo, T. P. Shields and J. K. Barton, *J. Am. Chem. Soc.*, 1993, **115**, 3877; (*b*) A. H. Krotz, L. Y. Kuo and J. K. Barton, *Inorg. Chem.*, 1993, **32**, 5963; (*c*) C. Turro, D. B. Hall, W. Chen, H. Zuilhof, J. K. Barton and N. J. Turro, *J. Phys. Chem. A*, 1998, **102**, 5708; (*d*) B. P. Hudson and J. K. Barton, *J. Am. Chem. Soc.*, 1998, **120**, 6877.
7 A. M. Pyle, T. Morii and J. K. Barton, *J. Am. Chem. Soc.*, 1990, **112**, 9432.
8 F. R. Keene, *Coord. Chem. Rev.*, 1997, **166**, 121.
9 (*a*) B. J. Goodfellow, V. Félix, S. M. D. Pacheco, J. Pedrosa de Jesus and M. G. B. Drew, *Polyhedron*, 1997, **16**, 393; (*b*) B. J. Goodfellow,

S. M. D. Pacheco, J. Pedrosa de Jesus, V. Félix and M. G. B. Drew, *Polyhedron,* 1997, **16**, 3293; (*c*) T. M. Santos, B. J. Goodfellow, J. Madureira, J. Pedrosa de Jesus, V. Felix and M. G. B. Drew, *New J. Chem.*, 1999, **23**, 1015.
10 G. Deslongchamps, B. A. Murray and J. Rebek, *J. Am. Chem. Soc.*, 1993, **115**, 797; K. Guckian, B. A. Schweitzer, X.-F. Ren, C. J. Sheils, P. L. Paris, D. C. Tahmassebi and E. T. Kool, *J. Am. Chem. Soc.*, 1996, **118**, 8182; K. Guckian, B. A. Schweitzer, X.-F. Ren, C. J. Sheils, P. L. Paris, D. C. Tahmassebi and E. T. Kool, *J. Am. Chem. Soc.*, 2000, **122**, 2213.
11 (*a*) J. E. Dickeson and L. A. Summers, *Aust. J. Chem.*, 1970, **23**, 1023; (*b*) E. Amouyal, A. Homsi, J.-C. Chambron and J.-P. Sauvage, *J. Chem. Soc.*, *Dalton Trans.*, 1990, 1841; (*c*) C. Hiort, P. Lincoln and B. Nordén, *J. Am. Chem. Soc.*, 1993, **115**, 3448; (*d*) M. R. Arkin, E. D. A. Stemp, R. E. Holmlin, J. K. Barton, A. Hörmann, E. C. J. Olson and P. F. Barbara, *Science*, 1996, **273**, 475; (*e*) J. Fees, M. Ketterle, A. Klein and W. Kaim, *J. Chem. Soc.*, *Dalton Trans.*, 1999, 2595.
12 A. M. Pyle, E. C. Long and J. K. Barton, *J. Am. Chem. Soc.*, 1989, **111**, 4520.
13 J. G. Collins, T. P. Shields and J. K. Barton, *J. Am. Chem. Soc.*, 1994, **116**, 9840.
14 R. L. Blakeley and M. K. De Armond, *J. Am. Chem. Soc.*, 1987, **109**, 4895.
15 Z. Serna, M. G. Barandika, R. Cortés, M. K. Urtiaga and M. I. Arriortua, *Polyhedron*, 1998, **18**, 249.
16 M. J. Bloemink, H. Engelking, S. Karentzopoulos, B. Krebs and J. Reedijk, *Inorg. Chem.*, 1996, **35**, 619.
17 A. D. Q. Ferreira, A. Bino and D. Gibson, *Inorg. Chim. Acta*, 1997, **265**, 155.
18 (*a*) P. Belser, A. von Zelewsky and M. Zehnder, *Inorg. Chem.*, 1981, **20**, 3098; (*b*) A. M. Pyle and J. K. Barton, *Inorg. Chem.*, 1987, **26**, 3820; (*c*) H. Masui, A. B. P. Lever and P. R. Auburn, *Inorg. Chem.*, 1991, **30**, 2402; (*d*) R. A. Metcalfe and A. B. P. Lever, *Inorg. Chem.*, 1997, **36**, 4762; (*e*) E. Jandrasics, B. Kolp, J. A. Wolny, A. von Zelewsky, *Inorg. Chim. Acta*, 1998, **272**, 153; (*f*) T. Jüstel, J. Bendix, N. Metzler-Nolte, T. Weyhermüller, B. Nuber and K. Wieghardt, *Inorg. Chem.*, 1998, **37**, 35.
19 K. N. Mitra, S. Choudhury, A. Castiñeiras and S. Goswami, *J. Chem. Soc.*, *Dalton Trans.*, 1998, 2901.
20 H. Bock, R. Dienelt, H. Schodel and T. T. H. Van, *Struct. Chem.*, 1998, **9**, 279.
21 S. L. Wang, J. W. Richardson, S. J. Briggs, R. A. Jacobson and W. P. Jensen, *Inorg. Chim. Acta*, 1986, **111**, 67; S. Sommerer, W. P. Jensen and R. A. Jacobson, *Inorg. Chim. Acta*, 1990, **172**, 3; S. O. Sommerer, J. D. Baker, W. P. Jensen, A. Hamza and R. A. Jacobson, *Inorg. Chim. Acta*, 1993, **210**, 173.
22 F. H. Allen, J. E. Davies, J. J. Galloy, O. Johnson, O. Kennard, C. F. Macrae and D. G. Watson, *J. Chem. Inf. Comput. Sci.*, 1991, **31**, 204.
23 N. Marsich, A. Camus, F. Ugozzoli and A. Manotti Lanfredi, *Inorg. Chim. Acta*, 1995, **236**, 117.
24 F. A. Cotton, L. M. Daniels, G. T. Jordan IV and C. A. Murillo, *Polyhedron*, 1998, **17**, 589.
25 Complex $[Ru([9]aneS_3)(dpm)Cl]^+$ **4** crystallises in the monoclinic system, space group $P2_1/a$ with $a = 8.356(11)$, $b = 24.473(27)$, $c = 23.297(25)$ Å, $\beta = 93.59(1)°$. A final refinement of 290 parameters led to $R = 0.1585$ and $R' = 0.4129$ for 2634 observed reflections with $I > 2\sigma(I)$. Complex $[Ru([9]aneS_3)(dpk)Cl]^+$ **5** crystallises in the monoclinic system, space group $P2_1/a$ with $a = 22.909(25)$, $b = 7.613(10)$, $c = 15.264(18)$ Å, $\beta = 102.30(1)°$. A final refinement of 178 parameters led to $R = 0.1586$ and $R' = 0.4454$ for 908 observed reflections with $I > 2\sigma(I)$. M. G. B. Drew and V. Félix, unpublished results.
26 D. C. Craig, M. L. Scudder, W.-A. McHale and H. A. Goodwin, *Aust. J. Chem.*, 1998, **51**, 1131.
27 R. Chotalia, E. C. Constable, M. J. Hannon and D. A. Tocher, *J. Chem. Soc.*, *Dalton Trans.*, 1995, 3571.
28 R. S. Glass, G. S. Wilson and W. N. Setzer, *J. Am. Chem. Soc.*, 1980, **102**, 5068.
29 J. Beech, P. J. Gragg and M. G. B. Drew, *J. Chem. Soc.*, *Dalton Trans.*, 1994, 719.
30 M. Yamada, Y. Tanaka, Y. Yoshimoto, S. Kuroda and I. Shimao, *Bull. Chem. Soc. Jpn.*, 1992, **65**, 1006.
31 W. Paw and R. Eisenberg, *Inorg. Chem.*, 1997, **36**, 2287.
32 A. L. Canty and N. J. Minchin, *Aust. J. Chem.*, 1986, **39**, 1063.
33 I. P. Evans, A. Spencer and G. Wilkinson, *J. Chem. Soc.*, *Dalton Trans.*, 1973, 204.
34 C. Landgrafe and W. S. Sheldrick, *J. Chem. Soc.*, *Dalton Trans.*, 1994, 1885.
35 W. Kabsch, *J. Appl. Crystallogr.*, 1988, **21**, 916.
36 G. M. Sheldrick, SHELX 97, University of Göttingen, 1997.
37 (*a*) A. L. Spek, PLATON, A Multipurpose Crystallographic tool, Utrecht University, Utrecht, 1999; (*b*) CERIUS 2, version 4.0, Molecular Simulations Inc, San Diego, 1999.